Spectral stochastic uncertainty quantification in chemical systems

M T Reagan[1], H N Najm[1]†, B J Debusschere[1], O P Le Maitre[2], O M Knio[3] and R G Ghanem[3]

[1] Sandia National Labs, 7011 East Ave, MS 9051, Livermore, CA 94550, USA
[2] Université d'Evry Val d'Essonne, Evry, France
[3] The Johns Hopkins University, Baltimore, MD 21218, USA

Abstract. Uncertainty quantification (UQ) in the computational modeling of physical systems is important for scientific investigation, engineering design, and model validation. We have implemented an "intrusive" UQ technique in which (1) model parameters and field variables are modeled as stochastic quantities, and are represented using polynomial chaos (PC) expansions in terms of Hermite polynomials functions of Gaussian random variables, and (2) the deterministic model equations are reformulated using Galerkin projection into a set of equations for the time evolution of the field variable PC mode strengths. The mode strengths relate specific parametric uncertainties to their effects on model outputs. In this work, the intrusive reformulation is applied to homogeneous ignition using a detailed chemistry model through the development of a reformulated pseudo-spectral chemical source term. We present results analyzing the growth of uncertainty during the ignition process. We also discuss numerical issues pertaining to the accurate representation of uncertainty with truncated PC expansions, and ensuing stability of the time integration of the chemical system.

AMS classification scheme numbers: 60G99, 65C20, 33C45

Submitted to: *Combust. Theory Modelling*

† Author to whom correspondence should be addressed. hnnajm@ca.sandia.gov

1. Introduction

Confidence intervals on predicted system behavior are necessary for design and optimization of engineering systems. They are also useful from a scientific point of view, where model validation with respect to experimental measurements requires careful measures of uncertainty in both experimental data and computational predictions. In general, uncertainty in computational results can be due to both model and parametric uncertainty. The present work deals with the latter. Empirical physical parameters used in the construction of computational models are inherently uncertain as a result of unavoidable experimental measurement errors. We seek to develop techniques to quantify propagation of this parametric uncertainty, with a focus on detailed, stiff, chemical kinetics.

In general, the propagation of parametric uncertainty can be studied using Monte Carlo (MC) simulations by sampling assumed or known distributions of model parameters over many iterations. For complex models that consume considerable computational resources, this method may be very costly and inefficient. Also, this approach does not readily provide information about the sensitivity of model outputs to specific parametric uncertainties. Further, conventional sensitivity analysis sheds some light on first-order parametric dependencies, but does not propagate nonlinear interactions through the model of interest.

An alternative approach is discussed here, based on a spectral stochastic description of uncertain parameters and field quantities using polynomial chaos (PC) expansions for stochastic representation of uncertainty. The polynomial chaos [1–7] is a member of the set of homogeneous chaos, first defined by Wiener [1]. Ghanem and Spanos [7] implemented a spectral PC expansion in terms of Hermite polynomials of Gaussian basis functions in a finite element method. This was applied in the modeling of transport in porous media [8], solid mechanics [9, 10] and structural [11] applications. The utility of the Hermite-Gaussian PC for modeling non-Gaussian processes was also investigated in [12, 13]. Le Maître *et al.* [14, 15] extended the application of these techniques to thermo-fluid applications in the context of low Mach number flow. Xiu *et al.* [16] used generalized PC [17] for stochastic UQ in the modeling of flow-structure interactions, and for diffusion problems [18]. Debusschere *et al.* [19,20] used PC for UQ applied to electrochemical flow in microfluidic systems. Reagan *et al.* [21] studied UQ for chemically reacting H_2-O_2 systems in supercritical water.

In the most basic application, using MC sampling of the stochastic parameters, the corresponding solutions of the deterministic system are evaluated and projected onto the PC basis to compute the spectral mode coefficients. These coefficients are then used to construct probability density functions (PDFs) of the solution, to infer sensitivity to various parametric uncertainties, and to highlight the dominant sources of uncertainty. This non-intrusive spectral projection (NISP) approach [11, 15, 21] has the advantage of being applicable to legacy codes, which are run with varying parameters to compute the statistics and spectral mode values.

For computationally intensive problems, large-scale Latin-Hypercube MC sampling [22] of many deterministic runs may not be practical. For example, studying homogeneous ignition using a reduced model of 8 uncertain reaction rate preexponentials and five uncertain

enthalpies of formation, requires over to 20,000 individual deterministic evaluations of the model to adequately sample the full stochastic space and reach convergence [21]. Increasing the order of the PC expansion to more accurately represent the resultant output PDFs and/or study larger sets of uncertain parameters can dramatically increase the number of samples required. More complex models containing a greater number of reactions increase both the required sampling and the time required to compute individual realizations. As a result, more complex problems demand a more efficient approach.

An "intrusive" spectral/pseudospectral methodology allows the direct incorporation of spectral stochastic information into the basic formulation of the model. If it is possible to reformulate the governing equations for a particular problem, numerical efficiency can be gained by creating a purpose-built spectral code. In general, these implementations of spectral PC expansions involve (1) the introduction of a new stochastic dimension for each uncertain parameter in the problem, (2) the expansion of parameters and field quantities using PC in terms of these stochastic dimensions, (3) the substitution of these expansions in the governing equations and their reformulation using a Galerkin projection procedure into equations for the stochastic mode strengths, and (4) the solution of this larger system of equations and the reconstruction of the field quantities of the solution based on their PC expansions in terms of the computed stochastic modes. Depending on system nonlinearities and the necessary spectral order, the computational effort required to solve this system can be many times smaller than that needed to generate the number of MC realizations required to yield uncertainty estimates of comparable accuracy.

It is important to note that, while polynomial chaos-based uncertainty quantification provides sensitivity information, it actually goes well beyond sensitivity analysis to propagate the full probablistic representation of the model inputs to the model outputs. Depending on the chosen order of the PC expansion, intrusive spectral methods also provide *higher-order* sensitivity information. Higher-order effects are not lumped into a single coefficient, but are considered independently and in terms of parameter-parameter interactions. This enables the analysis of uncertainties due to correlations between model parameters.

This paper advances the state of the art in UQ of chemical systems by developing the formulation for a spectral chemical source term for detailed chemical mechanisms with multiple parametric uncertainties in rate constants and thermodynamic properties. Further, we address the numerical challenges inherent in such an intrusive spetral stochastic construction for highly-nonlinear chemical systems. The application focus is on 0-D homogeneous ignition, a problem that highlights the utility and potential challenges of this approach. The treatment starts with a basic summary of spectral and pseudospectral reformulations, describes the components of the intrusive PC formulation for a generalized chemical source term, uses these tools to examine homegeneous ignition for a detailed reaction mechanism, examines the advantages and disadvantages of intrusively-reformulated models, and discusses issues of stability and the limits of the formulation.

2. Formulation

2.1. Spectral methodology

We describe an uncertain model parameter as a stochastic quantity with a known PDF. Let an uncertain parameter λ be empirically given by

$$\lambda = \overline{\lambda} \pm \hat{\lambda} \tag{1}$$

where $\overline{\lambda}$ is the mean and $\hat{\lambda}$ defines the range of empirical uncertainty.

With no additional information on the shape/moments of its distribution, we assume λ to be Gaussian with a mean λ_0 and a standard deviation λ_1 consistent with Eq. 1. Letting ξ denote a normalized Gaussian variable with zero mean and unit variance, λ can be expressed as:

$$\lambda = \lambda_0 + \xi\lambda_1 \tag{2}$$

If, on the other hand, additional physical constraints are in effect, e.g. when λ is a pre-exponential Arrhenius rate constant that is strictly positive, then a lognormal distribution is more adequate. In this case, as discussed in [12, 13] and section 2.3.4, λ can be expanded in powers of ξ, with the necessary order dictated by the skewness of the distribution.

For a general prescribed distribution of λ, satisfying specific conditions [23], we can represent λ as a spectral expansion in terms of suitable orthogonal eigenfunctions with weights associated with a particular density. A well-studied example is the Wiener process (Brownian motion) which can be written as a spectral expansion in terms of Hermite polynomials and a normal Gaussian distribution. Other examples include Charlier polynomials and the Poisson distribution, and the Laguerre polynomials and the Gamma distribution [23]. In the present context, these spectral expansions are generally referred to as Polynomial Chaos (PC) expansions, following Wiener [1], and focus will be exclusively on the Hermite-Gauss PC. Moreover, while these expansions are generally infinite series, this work will consider only PC expansions truncated at some suitably high order.

A parameter λ can be represented using the (truncated) PC expansion as,

$$\lambda = \sum_{k=0}^{P} \lambda_k \Psi_k \tag{3}$$

where the Ψ_k's are the orthogonal Hermite polynomial functions of ξ [7], such that

$$\Psi_k = \begin{cases} 1 & k = 0 \\ \xi & k = 1 \\ \xi^2 - 1 & k = 2 \\ \dots & \end{cases} \tag{4}$$

and the λ_k's are the known spectral mode strengths for the PC expansion for λ.

More generally, for N_{dim} uncertain parameters, each parameter introduces a stochastic dimension ξ, such that, with $\theta = \{\xi_1, \xi_2, \cdots, \xi_{N_{\text{dim}}}\}$,

$$\Psi_k = \Psi_k(\theta) = \Psi_k(\xi_1, \xi_2, ..., \xi_{N_{\text{dim}}}), \quad k = 0, \dots, P. \tag{5}$$

Up to second order ($N_{\text{ord}} = 2$), these polynomials are given by:

$$\Psi_k = \begin{cases} 1 & k = 0 \\ \xi_k & k = 1 \ldots N_{\text{dim}} \\ \xi_m \xi_n - \delta_{nm} & k = N_{\text{dim}} + 1 \ldots P;\ m, n = 1 \ldots N_{\text{dim}} \end{cases} \tag{6}$$

The Ψ_k's are orthogonal with respect to the inner product,

$$< \Psi_i \Psi_j > \equiv \int \cdots \int \Psi_i(\theta) \Psi_j(\theta) g(\xi_1) \cdots g(\xi_N) d\xi_1 \cdots d\xi_N \tag{7}$$

where

$$g(\xi) = \frac{e^{-\xi^2/2}}{\sqrt{2\pi}} \tag{8}$$

is the Gaussian measure. We thus have

$$< \Psi_i > = \delta_{i0}, \tag{9}$$

and

$$< \Psi_i \Psi_j > = 0, \quad i \neq j, \quad i > 0,\ j > 0 \tag{10}$$

Note that, in general [17], the number of terms in the PC expansion is given by: $P + 1 = (N_{\text{dim}} + N_{\text{ord}})/(N_{\text{dim}}! N_{\text{ord}}!)$

Using the above orthogonality, starting with the PC expansion for a general parameter λ in Eq. 3 above, multiplying both sides by Ψ_i and taking inner products, we have

$$\lambda_i = \frac{< \lambda \Psi_i >}{< \Psi_i^2 >}, \quad i = 0, \ldots, P \tag{11}$$

Using this formalism, a generic stochastic field variable $\Phi(x,t)$ can also be represented using the PC expansion, as:

$$\Phi = \sum_{k=0}^{P} \Phi_k(x,t) \Psi_k \tag{12}$$

where the Φ_k's are the *unknown* spectral modes of Φ, analogous to the known spectral modes of λ. Again, given the orthogonality of the Ψ_k's, the Φ_k's are given by

$$\Phi_k = \frac{\langle \Phi \Psi_k \rangle}{\langle \Psi_k^2 \rangle}, \quad k = 0, \ldots, P. \tag{13}$$

The projection in Eq. 13 can be used in non-intrusive UQ analysis [21] to determine the Φ_k's based on deterministic realizations corresponding to particular values of the random parameters. The Galerkin projection in Eq. 13 is also the basis for reformulating the governing equations. Such a reformulated model construction provides built-in spectral stochastic uncertainty information, and eliminates the need for extensive Monte Carlo sampling. Instead, the extended system of governing equations can be solved with an increase in computational load due to (1) an increase in the equation system size by a factor of $P + 1$, and (2) an increase in the cost of each equation right-hand-side evaluation due to coupling among the $P + 1$ modes.

For a simple example of full spectral reformulation, consider an ODE in terms of Φ and parameter λ:

$$\frac{d\Phi}{dt} = \lambda\Phi, \qquad \Phi(0) = \Phi_0 \tag{14}$$

We substitute the expansions Eq. 3 and Eq. 12 into the ODE, and rearrange to get:

$$\sum_{k=0}^{P} \frac{d\Phi_k}{dt}\Psi_k = \sum_{p=0}^{P}\sum_{q=0}^{P} \lambda_p \Phi_q \Psi_p \Psi_q \tag{15}$$

Multiplying both sides by Ψ_i, and taking inner products, using the orthogonality of the PC basis, we obtain:

$$\frac{d\Phi_i}{dt} = \sum_{p=0}^{P}\sum_{q=0}^{P} \lambda_p \Phi_q \frac{\langle \Psi_p \Psi_q \Psi_i \rangle}{\langle \Psi_i^2 \rangle}, \quad i = 0, \ldots, P \tag{16}$$

where the $C_{pqi} = \langle \Psi_p \Psi_q \Psi_i \rangle / \langle \Psi_i^2 \rangle$ are precomputed coefficient tensors.

Solving for the evolution of these modes allows the reconstruction of $\Phi(x,t)$ per Eq. 12. This approach requires extensive and specific recoding of an existing deterministic code, which can be difficult. For a nonlinear model with multiple stochastic parameters and field variables, evaluation of the multi-dimensional summations and coefficient tensors becomes intractable. Moreover, there is no evident means of dealing with non-polynomial functions of stochastic quantities within this fully spectral context. These difficulties are resolved using a pseudospectral construction, where order-2P PC expansions resulting from pairwise products of order-P stochastic quantities are reprojected onto an order-P polynomial before proceeding further. This retains the order-P accuracy of the construction, while providing great simplification of the implementation. This construction is discussed in the following section.

2.2. Pseudospectral formulation

In this formulation, a PC-product term involving more than two factors is evaluated using two-factor pseudospectral products. Consider for instance the triple product

$$w = \lambda u v \tag{17}$$

where λ, u, and v are expanded as in Eq. 3. Projecting each two-factor product onto a $(P+1)$ polynomial, we have:

$$\tilde{w} = uv \;\Rightarrow \tilde{w}_i = \sum_{j=0}^{P}\sum_{k=0}^{P} u_k v_j \frac{\langle \Psi_k \Psi_j \Psi_i \rangle}{\langle \Psi_i^2 \rangle} \tag{18}$$

$$w = \lambda\tilde{w} \Rightarrow w_i = \sum_{j=0}^{P}\sum_{k=0}^{P} \lambda_k \tilde{w}_j \frac{\langle \Psi_k \Psi_j \Psi_i \rangle}{\langle \Psi_i^2 \rangle} \tag{19}$$

This construction allows for a general representation using a new pseudospectral "overloaded" multiplication operation

$$w = \lambda * (u * v) \tag{20}$$

where each deterministic multiplication is transformed into a corresponding product of polynomial chaos expansions. This has great potential for automatic transformation of legacy deterministic code into a stochastic pseudo-spectral PC code. Note that the evaluation of the resulting pseudo-spectral mode strengths is straightforward for polynomial functions, $w(u)$, by addition of pseudospectral products, but requires additional work for other functions, such as inverses, exponentials, logarithms, etc. Generally, if a local polynomial approximation for any of these functions is found, at least in the $\pm 3\sigma(u)$ of u_0, then substitution of that polynomial in the above projection will give an approximation to the necessary w_a's. Taylor series expansions may be used towards this end, however, the resulting representation is not convergent in general, as dictated by the convergence of the Taylor series for the specific function at hand. Alternatively, the expectations can be evaluated using sampling or quadrature, but the associated computational cost rises very quickly with increasing number of stochastic dimensions ξ. Alternative approaches have been outlined in Debusschere *et al.* [20, 24]. Inverses, $w = 1/u$, can be handled robustly using a linear-system solve for the modes of w. We denote this pseudospectral inversion below as $w = 1 \oslash u$. Moreover, [24] presents a general integration approach for handling any function $w(u)$ as long as its derivative dw/du is a rational function of u. We have utilized these constructions to develop a a generalized library of routines for pseudospectral PC operations that multiplies, inverts, or otherwise algebraically transforms spectral variables.

2.3. Chemical source term

2.3.1. Definition of the chemical system A key to the construction of a spectral reacting-flow code is an efficient stochastic chemical source term. In the following, we present dimensionless deterministic and stochastic formulations for a chemical source term.

Consider a spatially homogeneous perfect gas mixture of N species χ_i, with $i = 1, \cdots, N$, participating in M reactions:

$$\sum_{i=1}^{N} \nu'_{ik} \chi_i \iff \sum_{i=1}^{N} \nu''_{ik} \chi_i, \quad k = 1, \ldots, M \tag{21}$$

where ν'_{ik} and ν''_{ik} are the stoichiometric coefficients for species i appearing as a reactant or product, respectively, in reaction k. Given this set of reactions, the mass production rate of species i is given by

$$w_i = W_i \sum_{k=1}^{M} \nu_{ik} C_k \mathcal{R}_k \tag{22}$$

where W_i is the molar mass of species i,

$$\nu_{ik} = \nu''_{ik} - \nu'_{ik} \tag{23}$$

and, C_k is a correction factor due to third-body and/or pressure-fall-off corrections [25]. This

factor is given by

$$\mathcal{C}_k = \begin{cases} 1 & \text{for a non-third-body, non-pressure-fall-off rxn} \\ \zeta_k = \sum_{i=1}^{N} \beta_{ik} c_i & \text{for a third-body, non-pressure-fall-off rxn} \\ \left(\frac{P_r^k}{P_r^k + 1} \right) F_k & \text{for a pressure-fall-off rxn (third body or not)} \end{cases} \tag{24}$$

where, β_{ik} is the third-body efficiency of species i in reaction k, P_r^k is given by [25]:

$$\mathrm{P}_r^k = \begin{cases} \frac{k_k^{F,0} c_M}{k_k^{F,\infty}} & \text{for a pressure-fall-off third-body (+M) rxn} \\ \frac{k_k^{F,0} c_i}{k_k^{F,\infty}} & \text{for a pressure-fall-off non-third-body (+}\chi_i\text{) rxn} \end{cases} \tag{25}$$

Here, c_M is the total concentration of the mixture, $k_k^{F,0}$ and $k_k^{F,\infty}$ are the low and high pressure forward rates of reaction k, respectively [25], and F_k is a known function of P_r^k and T describing fall-off behavior for each pressure fall-off reaction k [25]. $\mathcal{R}_k$ is the rate of progress of reaction k, given by

$$\mathcal{R}_k = k_k^F \prod_{i=1}^{N} c_i^{\nu'_{ik}} - k_k^R \prod_{i=1}^{N} c_i^{\nu''_{ik}} \tag{26}$$

where k_k^F and k_k^R are the forward and reverse rates of reaction k, $c_i = \rho Y_i / W_i$ is the molar concentration of species i, ρ is the mass-density of the mixture, and Y_i is the mass fraction of species i in the mixture.

The time-evolution of the chemical system is governed by the ODE system,

$$\frac{dc_i}{dt} = \frac{\mathrm{Da}}{W_i} w_i, \quad i = 1, \ldots, N-1 \tag{27}$$

$$\frac{d\rho}{dt} = \frac{\mathrm{Da}}{c_p T} \sum_{i=1}^{N} h_i w_i - \mathrm{Da} \overline{W} \sum_{i=1}^{N} \frac{w_i}{W_i} \tag{28}$$

with algebraic constraints resulting from mass conservation,

$$\sum_{i=1}^{N} Y_i = 1 \tag{29}$$

and the perfect gas state equation:

$$P_0 = \frac{\rho T}{\overline{W}} \tag{30}$$

In this nomenclature [26], Da is the Damköhler number defined based on reference quantities, T is the temperature, c_p is the mixture specific heat at constant pressure, h_i is the specific enthalpy of species i, P_0 is the stagnation pressure (assumed constant), $\overline{W} = 1/\sum_{i=1}^{N} Y_i W_i$ is the molar mass of the mixture. These equations are closed with initial conditions $c_i(t=0) = c_i^0$ and $\rho(t=0) = \rho^0$.

2.3.2. Fully spectral construction We illustrate in this section the necessary spectral construction for the representation of the reaction rates of progress, $\mathcal{R}_k$, given above in Eq.26, assuming known spectral expansions for the forward and reverse rates, and the concentrations. Moreover, we illustrate this for brevity with the forward term $\mathcal{R}_k^F$, given that the extension to the reverse term is straightforward in this context. Thus, we seek to present the full spectral construction for $\mathcal{R}_k^F$, given by

$$\mathcal{R}_k^F = k_k^F \prod_{i=1}^{N} c_i^{\nu'_{ik}}. \tag{31}$$

To begin with, in order to exclude zero exponents, define the set of species indices containing those species with non-zero stoichiometric coefficients on the reactants side of reaction k. This set is given by,

$$I_k = \{i | \nu'_{ik} \neq 0\} = \{i_1^k, i_2^k, \ldots, i_{L_k}^k\}. \tag{32}$$

Dropping the k-sub/super-scripts for clarity, we have

$$I = \{i_1, i_2, \ldots, i_L\} \tag{33}$$

and

$$\mathcal{R}^F = k^F \prod_{p=1}^{L} c_{i_p}^{\nu'_{i_p}} = k^F \prod_{p=1}^{L} \left(\sum_{j=0}^{P} (c_{i_p})_j \Psi_j \right)^{\nu'_{i_p}} \tag{34}$$

For any integer $n > 0$, we have

$$\left(\sum_{j=0}^{P} a_j \right)^n = \sum_{j_1=0}^{P} \sum_{j_2=0}^{P} \cdots \sum_{j_n=0}^{P} a_{j_1} a_{j_2} \cdots a_{j_n} = \sum_{j_b=0}^{P} \Bigg|_{b=1}^{n} \prod_{q=1}^{n} a_{j_q} \tag{35}$$

where

$$\sum_{j_b=0}^{P} \Bigg|_{b=1}^{n} \equiv \sum_{j_1=0}^{P} \sum_{j_2=0}^{P} \cdots \sum_{j_n=0}^{P} \tag{36}$$

so that $\mathcal{R}^F$ can be expressed as

$$\mathcal{R}^F = k^F \prod_{p=1}^{L} \sum_{j_b=0}^{P} \Bigg|_{b=1}^{\nu'_{i_p}} \prod_{q=1}^{\nu'_{i_p}} (c_{i_p})_{j_q} \Psi_{j_q}. \tag{37}$$

Further,

$$\begin{aligned} \mathcal{R}^F = k^F & \left(\sum_{(j_b)_1=0}^{P} \Bigg|_{b=1}^{\nu'_{i_1}} \prod_{q=1}^{\nu'_{i_1}} (c_{i_1})_{(j_q)_1} \Psi_{(j_q)_1} \right) \left(\sum_{(j_b)_2=0}^{P} \Bigg|_{b=1}^{\nu'_{i_2}} \prod_{q=1}^{\nu'_{i_2}} (c_{i_2})_{(j_q)_2} \Psi_{(j_q)_2} \right) \cdots \\ & \cdots \left(\sum_{(j_b)_L=0}^{P} \Bigg|_{b=1}^{\nu'_{i_L}} \prod_{q=1}^{\nu'_{i_L}} (c_{i_L})_{(j_q)_L} \Psi_{(j_q)_L} \right) \\ = & \sum_{(j_b)_1=0}^{P} \Bigg|_{b=1}^{\nu'_{i_1}} \sum_{(j_b)_2=0}^{P} \Bigg|_{b=1}^{\nu'_{i_2}} \cdots \sum_{(j_b)_L=0}^{P} \Bigg|_{b=1}^{\nu'_{i_L}} \prod_{p=1}^{L} \prod_{q=1}^{\nu'_{i_p}} (c_{i_p})_{(j_q)_p} \Psi_{(j_q)_p} \end{aligned} \tag{38}$$

or,

$$\mathcal{R}^F = k^F \sum_{(j_b)_z=0}^{P} \Big|_{b=1}^{\nu'_{i_z}} \Big|_{z=1}^{L} \left(\prod_{p=1}^{L} \prod_{q=1}^{\nu'_{i_p}} (c_{i_p})_{(j_q)_p} \right) \left(\prod_{p=1}^{L} \prod_{q=1}^{\nu'_{i_p}} \Psi_{(j_q)_p} \right) \tag{39}$$

Finally, with

$$k^F = \sum_{i=0}^{P} k_i^F \Psi_i \tag{40}$$

we have

$$\mathcal{R}^F = \sum_{i=0}^{P} \sum_{(j_b)_z=0}^{P} \Big|_{b=1}^{\nu'_{i_z}} \Big|_{z=1}^{L} \left(k_i^F \prod_{p=1}^{L} \prod_{q=1}^{\nu'_{i_p}} (c_{i_p})_{(j_q)_p} \right) \left(\Psi_i \prod_{p=1}^{L} \prod_{q=1}^{\nu'_{i_p}} \Psi_{(j_q)_p} \right) \tag{41}$$

and the mode strengths in the PC expansion for $\mathcal{R}^F = \sum_{a=0}^{P} \mathcal{R}_a^F \Psi_a$ are given by

$$\mathcal{R}_a^F = \sum_{i=0}^{P} \sum_{(j_b)_z=0}^{P} \Big|_{b=1}^{\nu'_{i_z}} \Big|_{z=1}^{L} \left(k_i^F \prod_{p=1}^{L} \prod_{q=1}^{\nu'_{i_p}} (c_{i_p})_{(j_q)_p} \right) \frac{\left\langle \Psi_a \Psi_i \prod_{p=1}^{L} \prod_{q=1}^{\nu'_{i_p}} \Psi_{(j_q)_p} \right\rangle}{\langle \Psi_a^2 \rangle} \tag{42}$$

It should be evident that proceeding in this manner is not only cumbersome but computationally intractable. This is a result of (1) the high-dimensional summation and product operations; (2) the fact that both the forward and reverse rates have complex dependencies on the presumed uncertainties in the reaction rate constants (preexponential, temperature exponent, and activation energy), field variables (temperature and concentrations), and thermodynamic properties; and (3) the necessary accounting for third body and pressure-falloff corrections. This is the primary motivation for the pseudospectral construction introduced above, and further specified below.

In the following, we discuss the dependence of the reaction rates on uncertain thermodynamic properties, and the specification of lognormal distributions for uncertain reaction rate parameters. Given this, we then proceed to the complete pseudo-spectral formulation for the chemical source term.

2.3.3. Reaction rates with thermodynamic uncertainties The generalized source term allows any rate constant k_j^F be uncertain. Consider a situation with several species $i = 1,\ldots,N$ participating in M reactions $k = 1,\ldots,M$ with forward rates $k_k^F = B_k T^{\alpha_1} e^{-E_k/T}$. The reverse rate is derived from the forward rate by a mutual relationship to the equilibrium constant. There may be instances where the mechanism specifies the reverse rate explicitly. If this is not the case, we must derive the spectral reverse reaction rate from the spectral forward rate constant. This coupling of forward and reverse reaction rates allows the introduction and propagation of thermodynamic parametric uncertainty into the source term.

The reverse rate is related to the forward rate through the equilibrium constant:

$$k_k^R = \frac{k_k^F}{K_{c,k}} \tag{43}$$

where $K_{c,k}$ is defined as:

$$K_{c,k} = \frac{e^{-\zeta_k/T}}{T^{\sigma_k}} \tag{44}$$

$$\sigma_k = \sum_{i=1}^{N} \nu_{ik} \tag{45}$$

$$\zeta_k = \sum_{i=1}^{N} \nu_{ik} g_i W_i \tag{46}$$

Note that $g_i = g_i(T) = h_i - Ts_i$ is the dimensionless Gibbs free energy per unit mass of species i.

The relationship between enthalpic and entropic uncertainties and the Gibbs free energy derives from the species heat capacity, $C_{p,i}$. Note that $g_i W_i = \overline{G_i^o} = G_i^o / RT_{ref}$ is the dimensionless per-mole Gibbs free energy, with G_i^o being the corresponding dimensional quantity. We recall that

$$G_i^o = H_i^o - TS_i^o \tag{47}$$

Assuming ideal gas properties, one can compute the enthalpy and entropy by integration over T:

$$H_i^o = \int_0^T C_{p,i} dT \tag{48}$$

$$S_i^o = \int_0^T \frac{C_{p,i}}{T} dT \tag{49}$$

Let $C_{p,i} = C_{p,i}(T)$ be uncertain with a specified mean $C_{p,i0}$ and standard deviation $C_{p,i1}$,

$$C_{p,i} = C_{p,i0} + \xi_i C_{p,i1} \tag{50}$$

where $C_{p,i0} = C_{p,i0}(T)$ and $C_{p,i1} = C_{p,i1}(T)$ are known functions of temperature and ξ_i is a Gaussian random variable. Integrating to compute the enthalpy and entropy:

$$H_i^o = \int_0^T C_{p,i0} dT + \xi_i \int_0^T C_{p,i1} dT \tag{51}$$

$$= H_{i0} + \xi_i H_{i1} \tag{52}$$

$$S_i^o = \int_0^T \frac{C_{p,i0}}{T} dT + \xi_i \int_0^T \frac{C_{p,i1}}{T} dT \tag{53}$$

$$= S_{i0} + \xi_i S_{i1} \tag{54}$$

Reconstituting the definition of G_i^o, we have

$$G_i^o = H_{i0} + \xi_i H_{i1} - T\left(S_{i0} + \xi_i S_{i1}\right) \tag{55}$$

$$= H_{i0} - TS_{i0} + \xi_i \left(H_{i1} - TS_{i1}\right) \tag{56}$$

Substituting $\Psi_i = \xi_i$ (first-order modes in a Gaussian basis) and $\Psi_0 = 1.0$ gives a complete expression representing G_i^o in terms of the means and standard deviations of enthalpy and entropy:

$$G_i^o = \left(H_{i0} - TS_{i0}\right)\Psi_0 + \left(H_{i1} - TS_{i1}\right)\Psi_i \tag{57}$$

$$= \sum_{m=0}^{1} \left(H_{im} - TS_{im}\right)\Psi_{m \cdot i} \tag{58}$$

G_i^o is defined here in molar units, and so we can divide by $G_{\text{ref}} = RT_{\text{ref}}$ to nondimensionalize, and substitute into Eq. 46:

$$\zeta_k = \sum_{i=1}^{N} \frac{\nu_{ik}}{RT_{\text{ref}}} \sum_{m=0}^{1} (H_{ik} - TS_{ik})\, \Psi_{m\cdot i} \tag{59}$$

$$= \sum_{m=0}^{1} \sum_{i=1}^{N} \frac{\nu_{ik}}{RT_{\text{ref}}} (H_{ik} - TS_{ik})\, \Psi_{m\cdot i} \tag{60}$$

This defines an uncertain $K_{c,k}$ in terms of uncertain thermodynamic parameters, coupling uncertainty in reaction equilibrium to uncertainty in the Gibbs free energy.

2.3.4. Lognormal distributions in a Gaussian basis When assuming *a priori* the probability distribution corresponding to each uncertain reaction rate pre-exponential constant, it is necessary to choose distributions with zero probability of negative values. One typical choice is the lognormal distribution [27]. We discuss here the means of construction of a PC expansion for a random variable with a given lognormal distribution.

Let g be a normal random variable with mean μ_g and standard deviation σ_g. Further, let u be a lognormal random variable [28], with

$$u = e^g \tag{61}$$

Then for a given $\zeta > 0$,

$$P[u \le \zeta] = P[g \le \ln \zeta] \tag{62}$$

Let the median of u be m_u, i.e. $P[u \le m_u] = 0.5$. Then, since $P[g \le \mu_g] = 0.5$, we have

$$\mu_g = \ln m_u \tag{63}$$

Following Phenix *et al.* [27], we can define a multiplicative factor, S, as

$$P[m_u/S \le u \le m_u S] = 1 - \varepsilon \tag{64}$$

where ε is a suitably small number (e.g. 0.05). then

$$\begin{aligned} 1 - \varepsilon &= P[u \le m_u S] - P[u \le m_u/S] = P[g \le \ln(m_u S)] - P[g \le \ln(m_u/S)] \\ &= P[g \le \mu_g + \ln S] - P[g \le \mu_g - \ln S] \\ &= 1 - P[g \ge \mu_g + \ln S] - P[g \le \mu_g - \ln S] \end{aligned} \tag{65}$$

But, by the symmetry of g, $P[g \ge \mu_g + \ln S] = P[g \le \mu_g - \ln S]$, hence

$$P[g \le \mu_g - \ln S] = \frac{\varepsilon}{2} \tag{66}$$

and

$$P[g \le \mu_g + \ln S] = 1 - \frac{\varepsilon}{2}. \tag{67}$$

With U denoting the standard normal random variable, we have

$$P[g \le \beta] \equiv F_g(\beta) = F_U\left(\frac{\beta - \mu_g}{\sigma_g}\right) \equiv P\left[U \le \frac{\beta - \mu_g}{\sigma_g}\right] \tag{68}$$

thus,

$$P[g \leq \mu_g + \ln S] = F_U(\frac{\ln S}{\sigma_g}) = 1 - \frac{\varepsilon}{2} \tag{69}$$

and, from tabulated F_U, we have,

$$\frac{\ln S}{\sigma_g} = F_U^{-1}(1 - \frac{\varepsilon}{2}) \tag{70}$$

or,

$$\sigma_g = \frac{\ln S}{F_U^{-1}(1 - \frac{\varepsilon}{2})} \tag{71}$$

such that, e.g. for $\varepsilon = 0.05$, we have $F_U^{-1}(1 - \frac{\varepsilon}{2}) = 1.96$.

Thus, given a presumed lognormal distribution for the random variable u, with known median m_u and multiplicative factor S, the corresponding normally distributed random variable g, such that $u = e^g$, is determined by its mean μ_g and standard deviation σ_g given in 63 and 71 above, respectively. Given this, Ghanem [12] provides the requisite formulation for the mode strengths of the sought-after PC expansion for u, where the k-th order spectral mode strength of u is given by:

$$u_k = \exp[\mu_g + \frac{1}{2}\sigma_g^2]\frac{\sigma_g^k}{k!}. \tag{72}$$

2.3.5. Assembling a pseudospectral source term As seen in the example of full-spectral reformulation, the evaluation of the products of multiple PC expansions can be quite complex. But by truncating the expansions of products to order P (section 2.2), a set of pseudospectral operators may be used to form the chemical source term.

First, define an overloaded product operator:

$$w = \prod_{i=1}^{N} {}^i u \approx \widetilde{w} = \prod_{i=1}^{N} {}^i u = (\cdots(({}^1u * {}^2u) * {}^3u) * \cdots * {}^N u) \tag{73}$$

Using pseudospectral operators, the spectral source term can be constructed directly, following the definition in section 2.3.1.

First, the forward reaction rate for each reaction,

$$k_k^F = B_k T^n e^{\frac{-E_a}{T}} \tag{74}$$

can be written in terms of pseudospectral multiplication, inversion, exponentiation, and logarithm operators:

$$k_k^F = B_k * (\exp[n * \ln(T) - E_a * (1 \oslash T)]) \tag{75}$$

where T is now a PC expansion for temperature, and B_k, n, and E_a are represented as PC expansions, introducing any specified parametric uncertainty.

Each reaction rate now includes the uncertainty contributed by an uncertain temperature (propagated in the computations), the parametric uncertainty that may be associated with a lognormally-distributed reaction pre-exponential, B_k, the parametric uncertainty in the

activation energy, and/or parametric uncertainty in the temperature exponent n (each as specified).

The reverse rate can be calculated in two ways. If an explicit reverse reaction rate is available, it can be included directly. Otherwise, the reverse reaction rate may be calculated from the equilibrium constant:

$$\frac{k_k^F}{k_k^R} = K_{c,k} = \frac{e^{-\zeta_k(T)/T}}{T^{\sigma_k}} \tag{76}$$

with ζ_k and σ_k as defined in Eqs. 43-46, T given by its computed PC expansion, and the requisite pseudospectral operations. This computation also includes the effect of uncertain temperature itself, along with the derived uncertainty in Gibbs free energies, $g_i(T)$, due to dependence on the uncertain temperature.

The truncated stochastic expansion for the rate of progress of reaction k, $\mathcal{R}_k$, in terms of pseudospectral exponentiation operators $(**)$ is given by

$$\mathcal{R}_k = k_k^F * \prod_{i=1}^{N} c_i ** \nu'_{ik} - k_k^R * \prod_{i=1}^{N} c_i ** \nu''_{ik} \tag{77}$$

At this stage, third-body efficiencies may be added pseudospectrally (Eq. 24), with $\mathcal{C}_k = 1$ for no correction and

$$\mathcal{C}_k = \sum_{i=1}^{N} (\beta_{ik} * c_i) \tag{78}$$

for third-body corrections with no pressure fall-off. The implementation of pressure fall-off corrections follows in a very similar manner using pseudo-spectral operations.

The mass production rate $(\mathrm{kg\,m^{-3}\,s^{-1}})$ of species i is now written generally as

$$w_i = W_i \sum_{k=1}^{M} \nu_{ik} * \mathcal{C}_k * \mathcal{R}_k \tag{79}$$

where w_i is a full stochastic expansion:

$$w_i = \sum_{k=1}^{P} w_{ik} \Psi_k \tag{80}$$

This approach has been implemented in the form of a pseudospectral chemistry library that accepts a local chemical state vector and computes a spectral stochastic rate-of-progress for each reaction, based on the PC expansions for temperature and concentrations and the parametric uncertainty associated with enthalpies of formation, activation energies, exponents, and reaction preexponentials. This library returns a full PC expansion of the chemical source term for each individual species.

2.3.6. Extended ODE system Returning to the governing equations for the chemical system, we write the PC expansions for concentrations, c_i, density, ρ, and temperature, T, as:

$$c_i(t) = \sum_{k=0}^{P} c_{ik}(t) \Psi_k, \quad i = 1, \ldots, N \tag{81}$$

$$\rho(t) = \sum_{k=0}^{P} \rho_k(t)\Psi_k \tag{82}$$

$$T(t) = \sum_{k=0}^{P} T_k(t)\Psi_k \tag{83}$$

and substitute into the corresponding chemical equations.

The time-evolution of the resulting pseudospectral chemical system is governed by the extended ODE system, for $k = 0,\ldots,P$:

$$\frac{dc_{ik}}{dt} = \frac{\mathrm{Da}}{W_i} w_{ik}, \quad i = 1,\ldots,(N-1) \tag{84}$$

$$\frac{d\rho_k}{dt} = \mathrm{Da}\sum_{i=1}^{N}\left\{[1 \oslash (c_p * T)] * (h_i * w_i)\right\}_k - \frac{\mathrm{Da}}{W_i}\sum_{i=1}^{N}\left(\overline{W} * w_i\right)_k \tag{85}$$

The new algebraic constraints derive from mass conservation for mode 0 of the expansion, given that all higher-order modes sum to zero, since mass is conserved with zero-uncertainty. Using the PC expansion

$$Y_i = \sum_{k=0}^{P} Y_{ik}\Psi_k \tag{86}$$

for Y_i, the mass fraction of species i, zero-uncertainty in mass conservation implies:

$$\sum_{i=1}^{N} Y_{i0} = 1, \tag{87}$$

$$\sum_{i=1}^{N} Y_{ik} = 0, \quad k = 1,\ldots,P \tag{88}$$

and finally, from the perfect gas state equation, where P_0 is the stagnation pressure and assumed to be constant, and uncertain,

$$P_0 = \left[(\rho * T) \oslash \overline{W}\right]_0 \tag{89}$$

$$0 = \left[(\rho * T) \oslash \overline{W}\right]_k, \quad k = 1,\ldots,P \tag{90}$$

These equations are closed with deterministic initial conditions:

$$c_{ik}(t=0) = \begin{cases} c_i^0 & k = 0 \\ 0 & k = 1,\ldots,P \end{cases} \tag{91}$$

$$\rho_k(t=0) = \begin{cases} \rho^0 & k = 0 \\ 0 & k = 1,\ldots,P \end{cases} \tag{92}$$

3. Results and discussion

3.1. Homogeneous ignition results

To demonstrate the solution of the above UQ ODE model, we focused on the homogeneous constant-temperature ignition of a hydrogen-air mixture with a detailed chemical mechanism [29]. Thus, we only integrate Eq. 84 along with the mass conservation

constraints (Eqs. 87 & 88). Initial conditions are deterministic, with T = 1200K, ρ = 0.276 kg/m^3, $c_{H_2} = 0.238 \times 10^{-5}$, $c_{O_2} = 0.119 \times 10^{-5}$, and $c_{N_2} = 0.832 \times 10^{-5}$. The integration proceeds at constant T and ρ. Physical properties, including the mean values of uncertain heats of formulation, were generated with the CHEMKIN properties database [25].

We specified two uncertain dimensions ($N_{\text{dim}} = 2$), and ran the integration with N_{ord} = 3, 5, and 7. We chose parametric uncertainties that reflect experimental estimates [27]. We model the uncertain preexponential Arrhenius rate constant for reaction 11 (HO_2 + H = OH + OH) as a lognormally distributed random variable, with a median value of 1.690×10^{14} mole-cm-sec-K and a multiplicative factor of 3.0. The second uncertain parameter is the enthalpy of OH, which we assume to have a normal distribution with a mean given by the deterministic CHEMKIN [25] data base and a standard deviation of 0.01 kcal/mole [21, 27].

The extended system of conservation equations with pseudospectrally-generated chemical source terms was integrated using the DVODE solver [30] with discrete numerical Jacobians. The integration used a timestep of 2×10^{-4} ms. For the complete integration, the mean and standard deviation calculated at each N_{ord} varied by less than 0.5%. The analysis in this section is based on results obtained with $N_{\text{ord}} = 5$.

Figure 1 shows the mean value of H_2O_2 concentration vs. time for the homogeneous ignition. Dashed lines indicate the range of resulting uncertainty with $\pm\sigma$ bounds. We observe a fast rise in both the mean H_2O_2 concentration and its standard deviation in the first 0.1 ms time interval. The resulting peak in uncertainty at $\approx$ 0.1 ms is a result of uncertainty in both the Rxn.11 rate constant and in the enthalpy of OH. At later time, there is a gradual decrease in uncertainty as the system tends towards equilibrium. We note that one expects the rate-constant uncertainty to have no impact at equilibrium, while the enthalpic uncertainty would be reflected in the equilibrated species mixture. This is in fact observed in the present results as shown in Fig. 3 below. The observation of this physically expected result from the present analysis based on truncated PC expansions provides validation of the computational predictions and suggests the adequacy of the chosen order of the expansion for the present problem.

Other radical species exhibit much larger uncertainties than H_2O_2. Figure 2 shows the mean value of HO_2 concentration vs. time, with $\pm\sigma$ bounds indicated. These results exhibit similar fast-rise in mean and standard deviation at early time, followed by a gradual decay to some asymptotically constant value of both at later time. Note the overall magnitude of total uncertainty in HO_2. Given realistic, moderate parametric uncertainties—uncertainties that reflect known limitations in the measurement of physical properties—the standard deviation of the concentration reaches over 40% of the mean. We note that the uncertainty in the H_2O product (not shown) is relatively small, while that associated with some intermediate species is evidently quite large in comparison.

A notable strength of the PC representation is that the contribution of specific parameters can be traced through each field quantity and into the simulation results. Figure 3 breaks down the 1^{st}-order contribution to the variance, σ^2, of the H_2O_2 concentration due to the two uncertain parameters. The shaded regions indicate the 1^{st}-order contribution of uncertainty

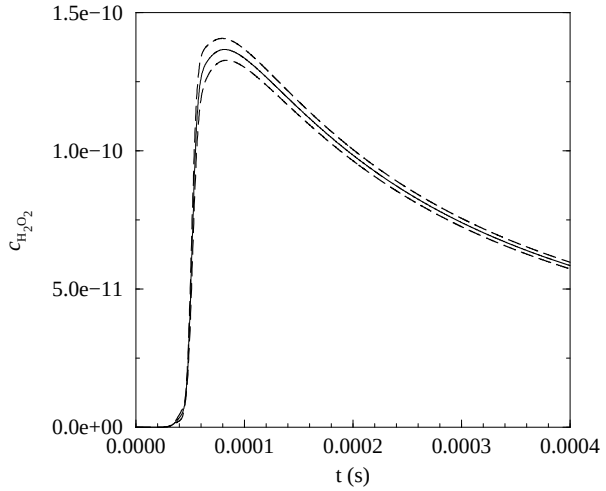

Figure 1. Time evolution of the mean (solid line) and ±σ-uncertainty bounds (dashed lines) in the concentration of H_2O_2.

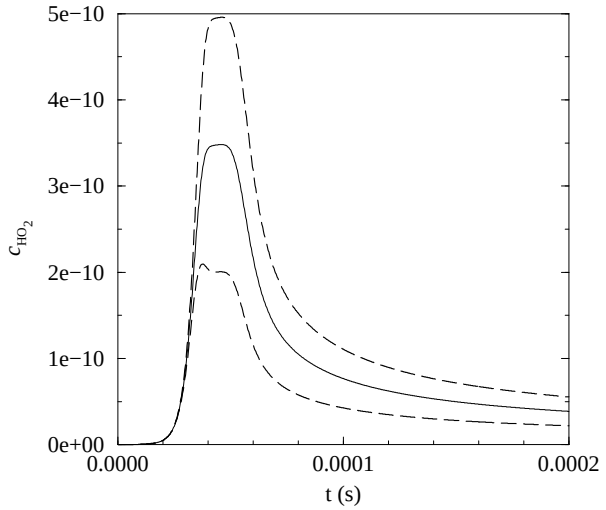

Figure 2. Time evolution of the mean (solid line) and ±σ-uncertainty bounds (dashed lines) in the concentration of HO_2.

from the uncertain enthalpy of formation, the 1^{st}-order contribution from the uncertain reaction preexponential, and the total variance calculated from the full expansion, include 2^{nd}, 3^{rd}, and higher-order effects. For these two uncertain parameters, the resulting concentration PDFs (not shown) are roughly Gaussian in form, and higher-order contributions are relatively small. This is consistent with the above comment on the adequacy of the 5^{th}-order truncated PC expansion for the present problem, and the accuracy of the present results in exhibiting the physically-expected negligible role of reaction-rate uncertainties near equilibrium. We note that other studies, which allowed for additional uncertain parameters [21], have shown larger contributions from higher orders. This form of analysis has great utility in larger and more complex systems, designating where and to what extent a given uncertainty affects

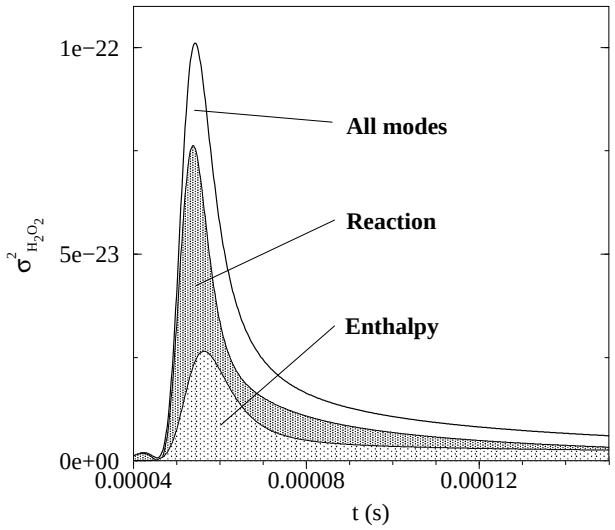

Figure 3. Decomposition of the uncertainty in the time-evolving computed variance of H_2O_2.

the total uncertainty in the predictions. This specifies which parameters are most impacted by experimental limitations, and thus may be used to guide future research. Also, since approximations and reductions are present in many chemical models, this methodology may reveal inherent limitations of mechanisms that may not be robust predictors of concentrations intermediate radical species.

3.2. Solvability of the pseudospectral formulation

A larger goal of this intrusive UQ construction is to construct large-scale reacting-flow simulation codes using pseudospectral stochastic PC operations. With this in mind, the solvability of the stiff chemistry may shed light into the numerical difficulties that may be encounted in more complex, highly-coupled multidimensional solvers. Two related effects are most apparent when assessing the solvability of the homogeneous ignition problem—the ability of the intrusive polynomial chaos approach to adequately represent the evolving probability distributions of the system variables, and the magnitude of the uncertainty.

Fig. 3.4 compares the PDFs of c_{HO_2} expanded to third, fifth, and seventh order at $t = 3.6 \times 10^{-5}$ s, using the pseudospectral source term, in the region of maximum uncertainty. The shape of the PDF is not skewed greatly from a Gaussian, but the standard deviation is considerable and the coefficient of variation, $\mathcal{C} = \sigma / c_i^0$, is accordingly quite large. There are clear discontinuities/spikes/artifacts in the PDF for $N_{\mathrm{ord}} = 3$ (solid line), indicating that, in the present case, third-order expansions do not adequately resolve the shape of the distribution. PDFs at $N_{\mathrm{ord}} = 5$ and 7 (circles and squares, respectively) show smoothly-varying nearly-identical distributions. Evidently, a fifth or seventh-order construction is necessary for accurate representation of the stochastic behavior in the present problem.

With the basic physical constraint of positive values for concentration, the resolution of the PDF near zero becomes important. Recall that the reformulation represents each

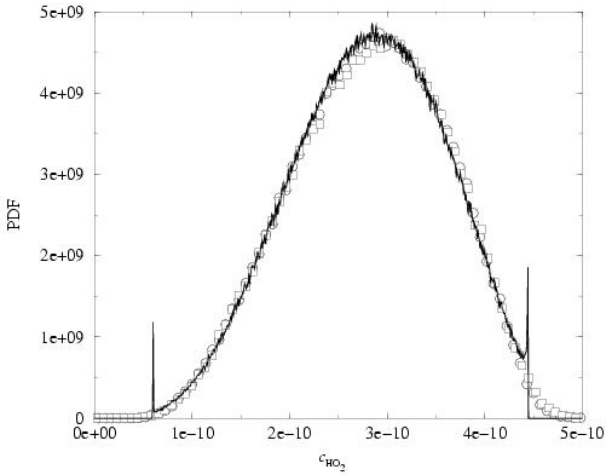

Figure 4. PDFs of HO_2 concentration at $t = 3.6 \times 10^{-5}$ s. The solid line represents $N_{\text{ord}} = 3$, the circles $N_{\text{ord}} = 5$, and the squares $N_{\text{ord}} = 7$

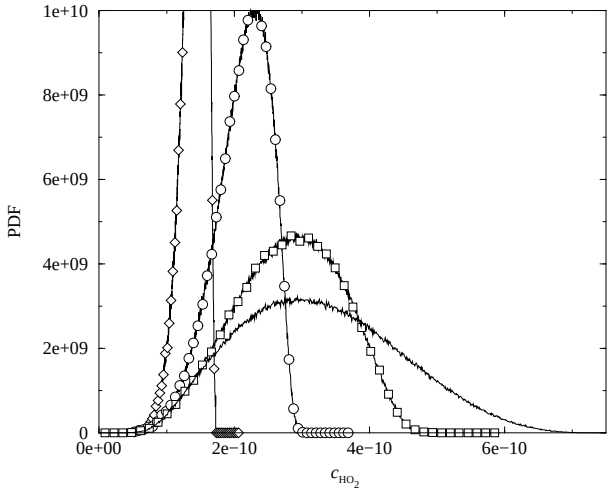

Figure 5. PDFs of HO_2 concentration at $t = 3.2 \times 10^{-5}$ s (diamonds), 3.4×10^{-5} s (circles), 3.6×10^{-5} s (squares), and 3.8×10^{-5} s (solid line). Results obtained with $N_{\text{ord}} = 5$.

random variable/process by a spectral PC expansion. While we do not discretize the PDF itself, a poorly-resolved expansion, i.e. one in which significant energy exists in the neglected/truncated higher order modes, will result in an unacceptable probability density. Expansions that are poorly resolved lead to large errors in the computed solution.

Figure 3.5 compares the PDF of c_{HO_2} at several points in the ignition process ($N_{\text{ord}} = 5$). As seen in Fig. 3.2, during the initial ignition, total uncertainty increases rapidly, with the standard deviation attaining a similar order-of-magnitude to the mean. When mode 1, which here dominates the standard deviation of the distribution, exceeds 30% of the mean, a steeply-varying PDF is required to insure no significant probability of negative c_{HO_2} values. As very large uncertainties develop, and σ approaches the mean, larger N_{ord} may be needed to compensate, and to adequately resolve the energy within the expansion. This increases the

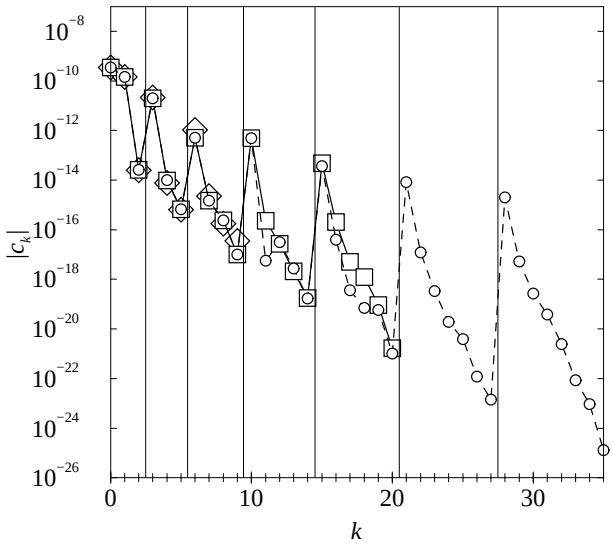

Figure 6. Absolute magnitude of $c_{HO_2}(k)$ modes at maximum total c_{HO_2} uncertainty for $N_{\text{ord}} = 3$ (diamonds), $N_{\text{ord}} = 5$ (squares), and $N_{\text{ord}} = 7$ (circles). Vertical lines separate orders from first through seventh.

complexity and the computational effort required to solve the problem.

Figure 3.6 illustrates the magnitude of mode strengths for HO_2 concentration for the PDF at $t = 3.8 \times 10^{-5}$ s, including expansions truncated at N_{ord} =3, 5, and 7. Vertical bars group the modes $|c_k|$ by order, from 1^{st} to 7^{th}. For $N_{\text{ord}} = 3$ and $N_{\text{ord}} = 5$, we see that some modes within the highest order bracket are greater in magnitude than the corresponding modes for the higher-order expansions. However, the trend of the modes in the log-linear plot indicates convergence. In this plot, the maximum and minimum mode amplitudes for each order correspond to modes dependent only on one of the uncertain dimensions. If we plot these mode amplitudes vs. N_{ord}, a roughly linear decay that suggests exponential convergence, with the maximum amplitudes (dependent on reaction uncertainty) converging more slowly than the minimum amplitudes (dependent on enthalpic uncertainty).

We note that the rate of decay of the energy/amplitude of the spectral modes with increasing order is a key indicator of the stability of the time integration of the PC system. In particular, if sufficiently large parametric uncertainties are chosen, then the growth in amplitude of higher-order modes can lead to a failure of the time integration procedure. To illustrate this, we performed another calculation of an extreme case. Using $N_{\text{ord}} = 5$, we set the pre-exponential of reaction 1 (H+O_2=O+OH) to be uncertain with $S = 1.5$ in addition to the previously-specified $S = 3.0$ for reaction 11. The enthalpic uncertainty was removed, leaving $N_{\text{dim}} = 2$. Figure 3.7 shows the PDFs of $c_{H_2O_2}$ at several times during the computation. The PDFs grow rapidly in width, with the standard deviation approaching the mean and signs of poor resolution for the PC expansions after 1.8×10^{-5} s. Analysis of the individual PC modes indicates that, once their decay rate with increasing order flattens, the values of the mode amplitudes diverge rapidly and the time integration fails. In Fig. 3.8, a plot of mean concentration and standard deviation vs. time is overlaid with individual 1^{st} and 2^{nd}-order

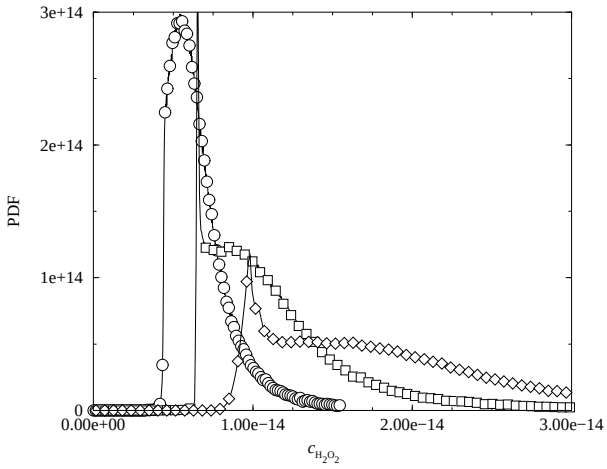

Figure 7. PDFs of H_2O_2 concentration at $t = 1.6 \times 10^{-5}$ s (circles), 1.8×10^{-5} s (squares), and 2.0×10^{-5} s (diamonds).

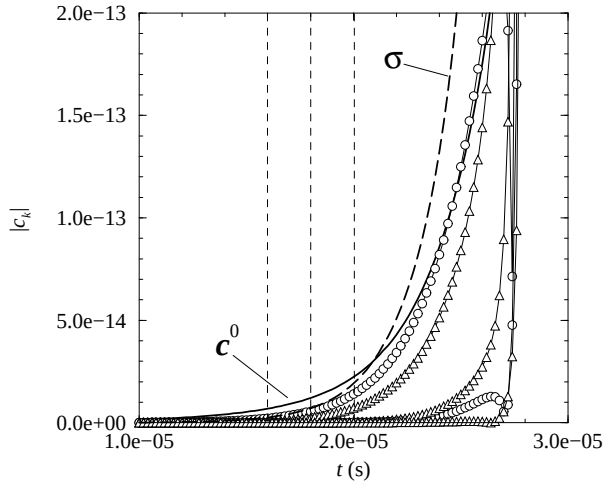

Figure 8. Evolution of $c_{H_2O_2}$ (solid line), first order $c_{H_2O_2}$ modes (circles), second-order $c_{H_2O_2}$ modes (triangles), and standard deviation (dashed line) vs. time. Vertical dashed lines correspond to the timesteps illustrated in the previous figure.

mode values. Note that for this 2-dimensional PC system there are two first-order modes and three second order modes, all of which are shown in the figure. Vertical dashed lines highlight the three time instances referenced in Fig. 3.7. By $t = 2.0 \times 10^{-5}$ s, the standard deviation has exceeded the mean, and both 1^{st} and 2^{nd}-order modes are growing rapidly, resulting in failure of the integration at $t = 2.75 \times 10^{-5}$ s. We note that increasing the order of the PC expansion merely leads to a delay in the onset of this instability.

Finally, we note that as the standard deviation increases, the behavior of the PDF tails around $c_i = 0$ can become an issue. If indeed the PC-reformulated system acts upon the full distribution of possible concentrations (as well as temperatures, densities, etc.), we should expect that finite probabilities of unphysical negative concentrations, generated by insufficiently resolved behavior near $c_i = 0$, will cause the integration to fail. This issue is

addressed below using a model initial value problem.

3.3. Model initial-value problem

To better understand the consequences of large standard deviations relative to the mean, i.e. a large coefficient of variation (COV), we considered a simpler case–the time integration of a model initial-value problem based on the chaos system. Specifically, we consider the ODE:

$$\frac{du}{dt} = g(u) = au(u+b)(u+c) \tag{93}$$

with $u(t=0) = U$. This system has two attractors, at $u = -b$ and $-c$. It also has a saddle point at $u = 0$. Using values of the constants of $b = 10$, $c = -1$, $a = -1$, any trajectory with $U > 0$ is attracted to the $u = 1$ limit, while $U < 0$ trajectories are attracted to $u = -10$. A trajectory with $U = 0$ remains at $u = 0$.

Now, allow u to be a stochastic quantity, $u = \sum_{k=0}^{P} u_k \Psi_k$, using fourth-order chaos $(P = 4)$, and let the constants a, b, c be deterministic as chosen. Further, assume that U is Gaussian with mean U_0 and standard deviation U_1. Thus, $U = U_0 + U_1\xi$, with zero higher order modes.

With fixed $U_1 = 0.08$, consider the behavior of $u_0(t)$ for two different values of $U_0 = 0.2, 0.3$. The corresponding PDFs for U are shown in Fig. 9. While both have non-zero probability of negative values–given the infinite support of the gaussian distribution, the case with $U_0 = 0.2$ has a larger COV, with corresponding larger probability of negative U. As Fig. 10 shows, the time evolution of u_0 is drastically different for the two cases. The initial stage of the evolution (up to $\sim t = 0.6$) is towards the positive attractor in both cases, with only minor difference in the trajectories. Soon after this however, the case with larger negative overlap is attracted towards the negative stationary point. The end result at $t = 1.5$ is that the two cases are stationary at the two attractors.

We note of course, that there is no sampling of either PDF in the time integration procedure. The equations integrated are the Galerkin-projected ODEs for the polynomial chaos expansion mode strengths. These equations are representing the physical situation accurately, thereby reflecting the increased probabilitiy of negative samples and its consequences. Also note that, despite the small probability of negative initial values, the mean of the PDF is completely dominated by their large magnitude as they tend towards -10, versus the much smaller values of the samples attracted to the positive limit.

We also note that, with an alternative problem, e.g. $du/dt = -10u(u-1)$, which has attractors at $u = 1$ and $-\infty$, the negative overlap of the PDF of U is a source of instability, as the negative branch of the solution tends to $-\infty$. The infinite well of this attractor creates a potential source of instability, as any overlap of the solution PDF with the region $u < 0$ would allow the solution to grow without bounds. A normally distributed initial condition can lead to an infinite rate of growth of the solution if its COV is large-enough.

Moreover, note that even the stable initial conditions in this discussion are in fact unstable if sufficiently high order is used for the PC expansion. For example, for the problem in Eq. 93, while using a 7^{th}-order expansion still gives the same final limit of 1.0 for u_0 in the $U_0 = 0.3$

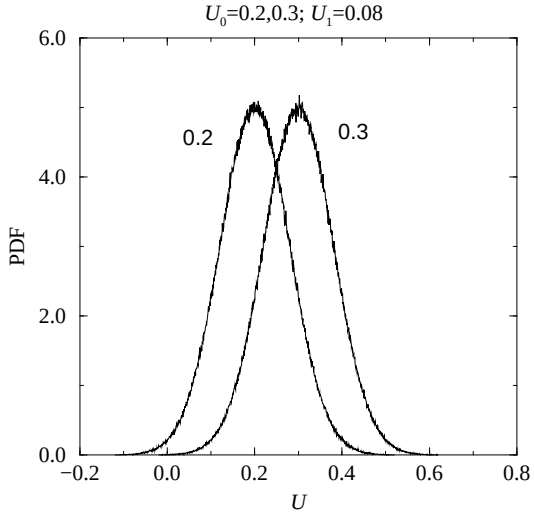

Figure 9. Two initial PDFs with $U_0 = 0.2$, and $U_0 = 0.3$, and $U_1 = 0.08$ in both cases. The PDF with the mean closer to zero overlaps the negative U region.

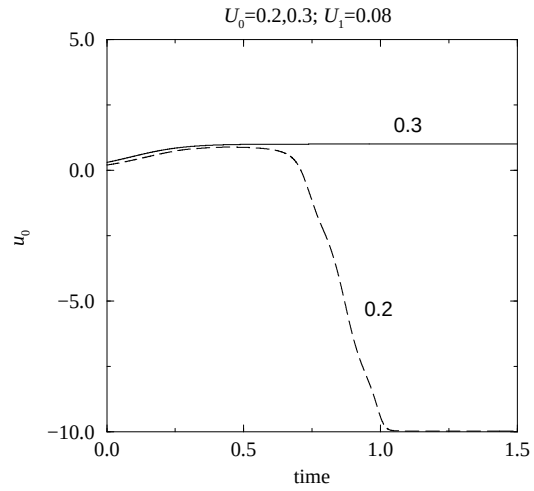

Figure 10. Evolution of u for each of the initial PDFs in Fig. 25, with $du/dt = au(u+b)(u+c)$ as defined above. The case with the initial PDF overlapping zero is attracted to the negative stationary point, in contrast to solution with an initial PDF that has much smaller overlap with zero.

case, taking the order up to 11 leads to u_0 heading into negative territory after first approaching 1.0. Possibly, the infinite support of the Gaussian PDF of the normally-distributed initial condition implies that, in the limit of infinite order, any such initial condition will tend to the negative limit. Thus, it is only the inaccuracy of the low-order expansions that prevents this from ocurring for some small COV values ($< 0.08/0.3$). Further work is necessary to adequately examine this conjecture.

It is also noteworthy that this same dependence on PC order and COV is observable with an initial condition U that is lognormally distributed. Thus, for example, we find that with a median U of 0.3, and a multiplicative factor $S_U = 4.5$, while both 4^{th} and 7^{th}-order reach

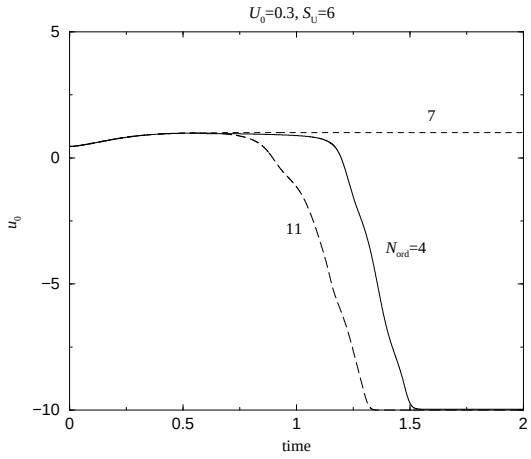

Figure 11. Evolution of u for a lognormal initial condition with increasing polynomial chaos order N_{ord}.

the positive limit and stay there within the 1.5 time limit, using 11^{th}-order chaos we find that u_0 leaves the 1.0 stationary point at around $t = 1.4$ and heads downward. Further, going to $S_U = 5.4$, we find that this occurs earlier at $t = 1$, and u_0 reaches the negative stationary point by $t = 1.5$. Moreover, with $S_U = 9$, even the 4^{th}-order solution leaves positive territory around t=0.5, and decreases towards -10. While this may seem surprising at first glance, given that the initial PDF ought-not to have any negative part, the explanation is based on the inadequate resolution of this and later PDFs by the truncated PC expansion. In the limit of very large S_U/U_0, or very low order, the truncated PC expansion for the lognormally distributed U exhibits an actual PDF that does have a finite probability of negative values. For example, for $S_U = 9$, the 4^{th}-order PDF of U has significant probabilities of negative values. This is not so at the lower S_U values ($S_U = 4.5 - 5.4$), where the initial PDFs are indeed well resolved with the PC expansions with order ≥ 4. However, the time integration procedure with the 11^{th}-order expansion leads to finite probabilities of negative $u(t)$ at early time, which evidently dominates the solution, driving u_0 to the negative limit. In fact, the results shown in Fig. 11, for $S_U = 6$, illustrate this situation very clearly. The results show that increasing the PC order from 4 to 7 leads to the stabilization of the solution at the positive attractor (at least up to $t = 2.0$). On the other hand, increasing the order further, to 11, leads back to an early departure of the solution from the positive limit.

Finally, it is important to examine clues for impending instability in the time integration due to such negative tails. Examining the system jacobian eigenvalue evolution does not give immediate clues to stability, as both the finite and infinite attractor problems exhibit rapidly-growing positive maximum eigenvalues for $\mathcal{C}_U > 0.3 - 0.4$. Additional analysis needs to be done to establish metrics for judging stability. This is investigated in the sections below.

3.4. PDF inversion

An interesting approach for detecting that a stochastic quantity u has a finite probability of being zero is to evaluate its stochastic inverse and examine the condition number of the matrix involved. This reveals one possible pathway to numerical difficulties—for example when part of the PDF for density, ρ, closely approaches zero, can we then expect to evaluate the stochastic inverse $T = 1/\rho$? In fact, this effect is observed during hydrogen-air ignition studies—the T expansion resulting from an inversion of density contains a small but finite probability of extremely large values. We present here the means of doing this check.

Note that we use a linear system solve to find the stochastic inverse, as outlined in [20, 31]. We outline that procedure here in order to explain the zero-crossing detection strategy. Thus, first, define the PC expansion for the random quantity u, and its inverse v,

$$u = \sum_{i=0}^{P} u_i \Psi_i \tag{94}$$

$$v = \frac{1}{u} = \sum_{j=0}^{P} v_j \Psi_j. \tag{95}$$

Then, since $w = uv = 1$, we express the PC expansion for the product,

$$w = \sum_{q=0}^{P} w_q \Psi_q = uv = \sum_{j=0}^{P} \sum_{i=0}^{P} u_i v_j \Psi_i \Psi_j. \tag{96}$$

Using Galerkin projection, we express the coefficients of the expansion for w in terms of the coefficients u_i and v_j,

$$w_k = \sum_{j=0}^{P} \sum_{i=0}^{P} u_i v_j \frac{< \Psi_i \Psi_j \Psi_k >}{< \Psi_k^2 >} = \sum_{j=0}^{P} \sum_{i=0}^{P} u_i v_j C_{ijk} = \delta_{k0} \tag{97}$$

But, since $w_k = \delta_{k0}$, we have

$$\sum_{j=0}^{P} \sum_{i=0}^{P} u_i v_j C_{ij0} = 1 \tag{98}$$

$$\sum_{j=0}^{P} \sum_{i=0}^{P} u_i v_j C_{ijk} = 0 \qquad k = 1, \cdots, P \tag{99}$$

This is a $(P+1)$-dimensional system of linear equations for v_j, $j = 0, \cdots, P$, i.e.,

$$\mathbf{A}\mathbf{v} = \mathbf{b} \tag{100}$$

where

$$A_{kj} = \sum_{i=0}^{P} u_i C_{ijk} \quad k, j = 0, \cdots, P \tag{101}$$

and

$$b_k = \delta_{k0}, \quad k = 0, \cdots, P \tag{102}$$

Note that A_{kj} is simply a linear combination of the modes of u, and thus easily evaluated. We can thus compute the condition number of $\mathbf{A}$ (the ratio of its maximum and minimum

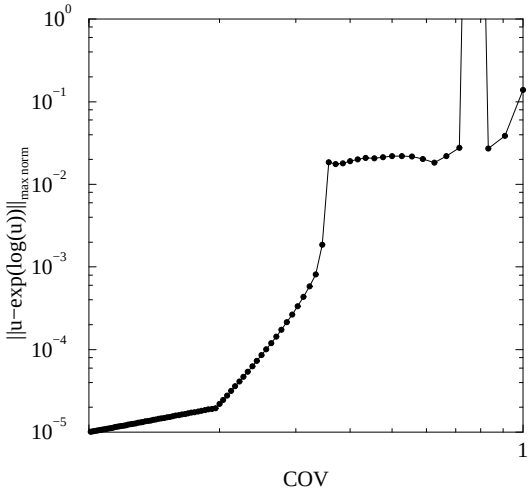

Figure 12. Computed error $||u - exp(log(u))||_\infty$ versus $\mathcal{C}_u$, where $u = \mathcal{N}(0.2/\mathcal{C}_u, 0.2)$ using fourth order chaos.

eigenvalues). Condition numbers of order 1 indicate a readily-invertable distribution, while larger condition numbers reflect potential difficulties with the inversion, and potential incidences of zero crossing in the PDF of u.

3.5. Detecting negative PDF tails

The stochastic natural logarithm function can be used to detect negative values in tails of distributions. Let u be a normal distribution, $u = \mathcal{N}(\sigma/\mathcal{C}_U, \sigma)$, then fix σ and vary the COV, $\mathcal{C}_U$. For each such choice of u, evaluate the error $\mathcal{E}$ given by

$$\mathcal{E} = ||u - \exp(\ln(u))||_\infty \tag{103}$$

The variation of E with COV is shown in Fig. 3.5. The error is small and smoothly varying for $\mathcal{C}_U < 0.36$. It also decays with decreasing $\mathcal{C}_U$. For $\mathcal{C}_U > 0.36$, however, the error is large, roughly fixed, and non-smooth. At large COVs, the PDF of u is wide enough to have $3\sigma > \mu$, leading to finite probability of negative u values. Clearly, the ln function evaluation with polynomial chaos will fail when the PDF has a significant negative tail. These results suggest the potential utility of the stochastic ln function for monitoring the solution during a time integration procedure, and providing early detection of signs of trouble. This information could be used to periodically filter the solution, sacrificing some measure of accuracy for stability.

4. Conclusions

We have implemented a pseudo-spectral stochastic uncertainty quantification scheme in the context of detailed chemical kinetics, allowing for uncertainties in thermodynamic properties and chemical rate constants. In this formulation, uncertainties are represented as stochastic variables, and are propagated accordingly through the computational model

using a polynomial chaos representation of simulated quantities. This is based on the use of spectral polynomial chaos expansions in terms of Hermite polynomial functions of Gaussian random variables for both uncertain parameters and solution field quantities, and on a Galerkin projection of the original deterministic governing equations onto the corresponding equations that govern the evolution of the spectral mode strengths of the unknowns. We outlined means of handling strictly positive lognormally distributed parameters, and of incorporation of equilibrium rate constants, reverse reactions, third body and pressure-falloff corrections, to arrive at a fully-reformulated ODE system for the chemical system.

We demonstrated this construction using a H_2-O_2 system for two uncertain parameters with prescribed uncertainties. The model amplified this parametric uncertainty considerably in the concentrations of some intermediate radicals. We outlined the strength of the present construction in providing information on the relative contributions of different parameters to the uncertainty in the solution of given field variables. These results suggest that the amplification of small parametric uncertainties may call into question the robustness of the chemical model for predicting certain radical species, and this observation highlights the importance of including uncertainty quantification in the computation. Moreover, these results are useful in pointing out specific rate constants where additional experimental measurements may assist in reducing uncertainty in model predictions.

A full, multiparameter analysis would include known uncertainties in all empirically-determined enthalpies of formation and reaction rate preexponentials. Future studies using this method will investigate the cumulative effects of such multi-parameter systems, particularly those including transport, focusing on the higher-order effects caused by the inherent coupling of the stochastic variables. This formulation preserves this non-linear coupling.

Limitations of the method include concerns about the resolution and adequate representation of the stochastic space when handling large uncertainties. For example, the constraint $c_j > 0$ within the chemistry integration may require high-order expansions (representing skewed or sharply-defined PDFs) to ensure stable expansions with a Hermite-Gaussian basis. Generally, the spectrum of "energy" in the polynomial chaos modes indicates impending trouble when the amplitudes of the high order modes grow, approaching those of low order modes. Resulting unphysical PDFs or poorly-resolved expansions may be corrected via the use of higher-order expansions, with the corresponding computational expense of solving a greater number of simultaneous equations. Our initial-value-problem model problem study suggests however that high-order, by itself, may not be sufficient for stability. Filtering of the PC expansions to decrease the amplitude of higher-order modes, and/or eliminate unphysical PDF tails, may be also necessary to stabilize the computations. In this regard, we presented two possible "error" measures, based on algebraic manipulations of the polynomial chaos modes, that may be used to infer impending signs of trouble in the PDF of a given variable. More work is required in this regard.

5. Acknowledgements

This work is supported through the Laboratory Directed Research and Development program at Sandia National Laboratories funded by the U.S. Department of Energy, and by the DOE Office of Basic Energy Sciences (BES), Division of Chemical Sciences, Geosciences and Biosciences.

6. References

[1] Wiener, N., *Amer. J. Math.*, 60:897–936 (1938).
[2] Cameron, R., and Martin, W., *Ann. Math.*, 48:385–392 (1947).
[3] Chorin, A., *J. Computational Phys.*, 8:472–482 (1971).
[4] Maltz, F., and Hitzl, D., *J. Computational Phys.*, 32:345–376 (1979).
[5] Meecham, W., and Jeng, D., *J. Fluid Mech.*, 32:225 (1968).
[6] Chorin, A., *J. Fluid Mech.*, 63:21–32 (1974).
[7] Ghanem, R., and Spanos, P., *Stochastic Finite Elements: A Spectral Approach*, Springer Verlag, New York, 1991.
[8] Ghanem, R., *Comput. Methods Appl. Mech. Engrg.*, 158:199–220 (1998).
[9] Ghanem, R., *Comput. Methods Appl. Mech. Engrg.*, 168:19–34 (1999).
[10] Ghanem, R., *ASCE J. Eng. Mech.*, 125:26–40 (1999).
[11] Ghanem, R., Red-Horse, J., and Sarkar, A., *8th ASCE Specialty Conference of Probabilistic Mechanics and Structural Reliability*, ASCE, 2000.
[12] Ghanem, R., *ASME J. Appl. Mech.*, 66(4):964–973 (1999).
[13] Sakamoto, S., and Ghanem, R., *ASCE J. Eng. Mech.*, 128(2):190–201 (2002).
[14] Le Maître, O., Knio, O., Najm, H., and Ghanem, R., *J. Comp. Phys.*, 173:481–511 (2001).
[15] Le Maître, O., Reagan, M., Najm, H., Ghanem, R., and Knio, O., *J. Comp. Phys.*, 181:9–44 (2002).
[16] Xiu, D., Lucor, D., Su, C.-H., and Karniadakis, G., *ASME J. Fluids Engineering*, 124:51–59 (2002).
[17] Xiu, D., and Karniadakis, G., *SIAM J. Sci. Comput.*, 24(2):619–644 (2002).
[18] Xiu, D., and Karniadakis, G., *Computer Methods in Applied Mechanics and Engineering*, 191:4927–4948 (2002).
[19] Debusschere, B., Najm, H., Matta, A., Shu, T., Knio, O., Ghanem, R., and Le Maître, O., *Proc.* 5^{th} *Int. Conf. on Modeling and Simulation of Microsystems*, 2002, , pp. 384–387.
[20] Debusschere, B., Najm, H., Matta, A., Knio, O., Ghanem, R., and Le Maître, O., *Phys. Fluids*, 15(8):2238–2250 (2003).
[21] Reagan, M., Najm, H., Ghanem, R., and Knio, O., *Combustion and Flame*, 132:545–555 (2003).
[22] McKay, M., Beckman, R., and Conover, W., *Technometrics*, 21:239–245 (1979).
[23] Schoutens, W., *Stochastic Processes and Orthogonal Polynomials*, Springer, 2000.
[24] Debusschere, B., Najm, H., Pebay, P., Knio, O., Ghanem, R., and Le Maître, O., *SIAM J. on Sci. Comp.* (2003) submitted.
[25] Kee, R., Rupley, F., and Miller, J., Sandia Report SAND89-8009B, Sandia National Labs., Livermore, CA, (1993).
[26] Najm, H., Wyckoff, P., and Knio, O., *J. Comp. Phys.*, 143(2):381–402 (1998).
[27] Phenix, B., Dinaro, J., Tatang, M., Tester, J., Howard, J., and McRae, G., *Combustion and Flame*, 112:132–146 (1998).
[28] Vanmarcke, E., *Random Fields: Analysis and Synthesis*, MIT Press, 1988.
[29] Yetter, R., Dryer, F., and Rabitz, H., *Combust. Sci. Technol.*, 79:97 (1991).
[30] Brown, P., Byrne, G., and Hindmarsh, A., *SIAM J. Sci. Stat. Comput.*, 10:1038–1051 (1989).
[31] Le Maître, O., Reagan, M., Debusschere, B., Najm, H., Ghanem, R., and Knio, O., *SIAM J. Scientific Computing* (2003) submitted.